Physics Letters B 813 (2021) 136059

Contents lists available at ScienceDirect

Physics Letters B

www.elsevier.com/locate/physletb

Observation of a resonant structure in $e^+e^- \to \omega\eta$ and another in $e^+e^- \to \omega\pi^0$ at center-of-mass energies between 2.00 and 3.08 GeV

BESIII Collaboration *

M. Ablikim [a], M.N. Achasov [j,4], P. Adlarson [bs], S. Ahmed [o], M. Albrecht [d], A. Amoroso [bp,br], Q. An [bm,ax], Y. Bai [aw], O. Bakina [ae], R. Baldini Ferroli [w], I. Balossino [y], Y. Ban [an,12], K. Begzsuren [ab], J.V. Bennett [e], N. Berger [ad], M. Bertani [w], D. Bettoni [y], F. Bianchi [bp,br], J. Biernat [bs], J. Bloms [bj], A. Bortone [bp,br], I. Boyko [ae], R.A. Briere [e], H. Cai [bt], X. Cai [a,ax], A. Calcaterra [w], G.F. Cao [a,be], N. Cao [a,be], S.A. Cetin [bb], J.F. Chang [a,ax], W.L. Chang [a,be], G. Chelkov [ae,2,3], D.Y. Chen [f], G. Chen [a], H.S. Chen [a,be], M.L. Chen [a,ax], S.J. Chen [al], X.R. Chen [aa], Y.B. Chen [a,ax], W. Cheng [br], G. Cibinetto [y], F. Cossio [br], X.F. Cui [am], H.L. Dai [a,ax], J.P. Dai [ar,8], X.C. Dai [a,be], A. Dbeyssi [o], R.B. de Boer [d], D. Dedovich [ae], Z.Y. Deng [a], A. Denig [ad], I. Denysenko [ae], M. Destefanis [bp,br], F. De Mori [bp,br], Y. Ding [aj], C. Dong [am], J. Dong [a,ax], L.Y. Dong [a,be], M.Y. Dong [a,ax,be], S.X. Du [bw], J. Fang [a,ax], S.S. Fang [a,be], Y. Fang [a], R. Farinelli [y,z], L. Fava [bq,br], F. Feldbauer [d], G. Felici [w], C.Q. Feng [bm,ax], M. Fritsch [d], C.D. Fu [a], Y. Fu [a], X.L. Gao [bm,ax], Y. Gao [bn], Y. Gao [an,12], Y.G. Gao [f], I. Garzia [y,z], E.M. Gersabeck [bh], A. Gilman [bi], K. Goetzen [k], L. Gong [am], W.X. Gong [a,ax], W. Gradl [ad], M. Greco [bp,br], L.M. Gu [al], M.H. Gu [a,ax], S. Gu [b], Y.T. Gu [m], C.Y. Guan [a,be], A.Q. Guo [v], L.B. Guo [ak], R.P. Guo [ap], Y.P. Guo [ad], Y.P. Guo [i,9], A. Guskov [ae], S. Han [bt], T.T. Han [aq], T.Z. Han [i,9], X.Q. Hao [p], F.A. Harris [bf], K.L. He [a,be], F.H. Heinsius [d], T. Held [d], Y.K. Heng [a,ax,be], M. Himmelreich [k,7], T. Holtmann [d], Y.R. Hou [be], Z.L. Hou [a], H.M. Hu [a,be], J.F. Hu [ar,8], T. Hu [a,ax,be], Y. Hu [a], G.S. Huang [bm,ax], L.Q. Huang [bn], X.T. Huang [aq], Z. Huang [an,12], N. Huesken [bj], T. Hussain [bo], W. Ikegami Andersson [bs], W. Imoehl [v], M. Irshad [bm,ax], S. Jaeger [d], S. Janchiv [ab,11], Q. Ji [a], Q.P. Ji [p], X.B. Ji [a,be], X.L. Ji [a,ax], H.B. Jiang [aq], X.S. Jiang [a,ax,be], X.Y. Jiang [am], J.B. Jiao [aq], Z. Jiao [r], S. Jin [al], Y. Jin [bg], T. Johansson [bs], N. Kalantar-Nayestanaki [ag], X.S. Kang [aj], R. Kappert [ag], M. Kavatsyuk [ag], B.C. Ke [as,a], I.K. Keshk [d], A. Khoukaz [bj], P. Kiese [ad], R. Kiuchi [a], R. Kliemt [k], L. Koch [af], O.B. Kolcu [bb,6], B. Kopf [d], M. Kuemmel [d], M. Kuessner [d], A. Kupsc [bs], M.G. Kurth [a,be], W. Kühn [af], J.J. Lane [bh], J.S. Lange [af], P. Larin [o], A. Lavania [u], L. Lavezzi [br], H. Leithoff [ad],

* *E-mail address:* besiii-publications@ihep.ac.cn.

[1] Also at Bogazici University, 34342 Istanbul, Turkey.

[2] Also at the Moscow Institute of Physics and Technology, Moscow 141700, Russia.

[3] Also at the Functional Electronics Laboratory, Tomsk State University, Tomsk, 634050, Russia.

[4] Also at the Novosibirsk State University, Novosibirsk, 630090, Russia.

[5] Also at the NRC "Kurchatov Institute", PNPI, 188300, Gatchina, Russia.

[6] Also at Istanbul Arel University, 34295 Istanbul, Turkey.

[7] Also at Goethe University Frankfurt, 60323 Frankfurt am Main, Germany.

[8] Also at Key Laboratory for Particle Physics, Astrophysics and Cosmology, Ministry of Education; Shanghai Key Laboratory for Particle Physics and Cosmology; Institute of Nuclear and Particle Physics, Shanghai 200240, People's Republic of China.

[9] Also at Key Laboratory of Nuclear Physics and Ion-beam Application (MOE) and Institute of Modern Physics, Fudan University, Shanghai 200443, People's Republic of China.

[10] Also at Harvard University, Department of Physics, Cambridge, MA, 02138, USA.

[11] Currently at: Institute of Physics and Technology, Peace Ave.54B, Ulaanbaatar 13330, Mongolia.

[12] Also at State Key Laboratory of Nuclear Physics and Technology, Peking University, Beijing 100871, People's Republic of China.

[13] School of Physics and Electronics, Hunan University, Changsha 410082, China.

https://doi.org/10.1016/j.physletb.2020.136059

M. Lellmann [ad], T. Lenz [ad], C. Li [ao], C.H. Li [ai], Cheng Li [bm,ax], D.M. Li [bw], F. Li [a,ax], G. Li [a], H.B. Li [a,be], H.J. Li [i,9], J.L. Li [aq], J.Q. Li [d], Ke Li [a], L.K. Li [a], Lei Li [c], P.L. Li [bm,ax], P.R. Li [ah], S.Y. Li [az], W.D. Li [a,be], W.G. Li [a], X.H. Li [bm,ax], X.L. Li [aq], Z.B. Li [ay], Z.Y. Li [ay], H. Liang [bm,ax], H. Liang [a,be], Y.F. Liang [au], Y.T. Liang [aa], L.Z. Liao [a,be], J. Libby [u], C.X. Lin [ay], B. Liu [ar,8], B.J. Liu [a], C.X. Liu [a], D. Liu [bm,ax],D.Y. Liu [ar,8], F.H. Liu [at], Fang Liu [a], Feng Liu [f], H.B. Liu [m], H.M. Liu [a,be], Huanhuan Liu [a], Huihui Liu [q], J.B. Liu [bm,ax], J.Y. Liu [a,be], K. Liu [a], K.Y. Liu [aj], Ke Liu [f], L. Liu [bm,ax], Q. Liu [be], S.B. Liu [bm,ax], Shuai Liu [av], T. Liu [a,be], X. Liu [ah], Y.B. Liu [am], Z.A. Liu [a,ax,be], Z.Q. Liu [aq], Y.F. Long [an,12], X.C. Lou [a,ax,be], F.X. Lu [p], H.J. Lu [r], J.D. Lu [a,be], J.G. Lu [a,ax], X.L. Lu [a], Y. Lu [a], Y.P. Lu [a,ax], C.L. Luo [ak], M.X. Luo [bv], P.W. Luo [ay], T. Luo [i,9], X.L. Luo [a,ax], S. Lusso [br], X.R. Lyu [be], F.C. Ma [aj], H.L. Ma [a], L.L. Ma [aq], M.M. Ma [a,be], Q.M. Ma [a], R.Q. Ma [a,be], R.T. Ma [be], X.N. Ma [am], X.X. Ma [a,be], X.Y. Ma [a,ax], Y.M. Ma [aq], F.E. Maas [o], M. Maggiora [bp,br], S. Maldaner [ad], S. Malde [bk], Q.A. Malik [bo], A. Mangoni [x], Y.J. Mao [an,12], Z.P. Mao [a], S. Marcello [bp,br], Z.X. Meng [bg], J.G. Messchendorp [ag], G. Mezzadri [y], T.J. Min [al], R.E. Mitchell [v], X.H. Mo [a,ax,be], Y.J. Mo [f], N.Yu. Muchnoi [j,4], H. Muramatsu [bi], S. Nakhoul [k,7], Y. Nefedov [ae], F. Nerling [k,7], I.B. Nikolaev [j,4], Z. Ning [a,ax], S. Nisar [h,10], S.L. Olsen [be], Q. Ouyang [a,ax,be], S. Pacetti [x], X. Pan [av], Y. Pan [bh], A. Pathak [a], P. Patteri [w], M. Pelizaeus [d], H.P. Peng [bm,ax], K. Peters [k,7], J. Pettersson [bs], J.L. Ping [ak], R.G. Ping [a,be], A. Pitka [d], R. Poling [bi], V. Prasad [bm,ax], H. Qi [bm,ax], H.R. Qi [az], M. Qi [al], T.Y. Qi [b], S. Qian [a,ax], W.-B. Qian [be], Z. Qian [ay], C.F. Qiao [be], L.Q. Qin [l], X.P. Qin [m], X.S. Qin [d], Z.H. Qin [a,ax], J.F. Qiu [a], S.Q. Qu [am], K.H. Rashid [bo], K. Ravindran [u], C.F. Redmer [ad], A. Rivetti [br], V. Rodin [ag], M. Rolo [br], G. Rong [a,be], Ch. Rosner [o], M. Rump [bj], A. Sarantsev [ae,5], M. Savrié [z], Y. Schelhaas [ad], C. Schnier [d], K. Schoenning [bs], D.C. Shan [av], W. Shan [s], X.Y. Shan [bm,ax], M. Shao [bm,ax], C.P. Shen [b], P.X. Shen [am], X.Y. Shen [a,be], H.C. Shi [bm,ax], R.S. Shi [a,be], X. Shi [a,ax], X.D. Shi [bm,ax], J.J. Song [aq], Q.Q. Song [bm,ax], W.M. Song [ac], Y.X. Song [an,12], S. Sosio [bp,br], S. Spataro [bp,br], F.F. Sui [aq], G.X. Sun [a], J.F. Sun [p], L. Sun [bt], S.S. Sun [a,be], T. Sun [a,be], W.Y. Sun [ak], Y.J. Sun [bm,ax], Y.K. Sun [bm,ax], Y.Z. Sun [a], Z.T. Sun [a], Y.H. Tan [bt], Y.X. Tan [bm,ax], C.J. Tang [au], G.Y. Tang [a], J. Tang [ay], V. Thoren [bs], B. Tsednee [ab], I. Uman [bd], B. Wang [a], B.L. Wang [be], C.W. Wang [al], D.Y. Wang [an,12], H.P. Wang [a,be], K. Wang [a,ax], L.L. Wang [a], M. Wang [aq], M.Z. Wang [an,12], Meng Wang [a,be], W.H. Wang [bt], W.P. Wang [bm,ax], X. Wang [an,12], X.F. Wang [ah], X.L. Wang [i,9], Y. Wang [bm,ax], Y. Wang [ay], Y.D. Wang [o], Y.F. Wang [a,ax,be], Y.Q. Wang [a], Z. Wang [a,ax], Z.Y. Wang [a], Ziyi Wang [be], Zongyuan Wang [a,be], T. Weber [d], D.H. Wei [l], P. Weidenkaff [ad], F. Weidner [bj], S.P. Wen [a], D.J. White [bh], U. Wiedner [d], G. Wilkinson [bk], M. Wolke [bs], L. Wollenberg [d], J.F. Wu [a,be], L.H. Wu [a], L.J. Wu [a,be], X. Wu [i,9], Z. Wu [a,ax], L. Xia [bm,ax], H. Xiao [i,9], S.Y. Xiao [a], Y.J. Xiao [a,be], Z.J. Xiao [ak], X.H. Xie [an,12], Y.G. Xie [a,ax], Y.H. Xie [f], T.Y. Xing [a,be], X.A. Xiong [a,be], G.F. Xu [a], J.J. Xu [al], Q.J. Xu [n], W. Xu [a,be], X.P. Xu [av], L. Yan [i,9], L. Yan [bp,br], W.B. Yan [bm,ax], W.C. Yan [bw], Xu Yan [av], H.J. Yang [ar,8], H.X. Yang [a], L. Yang [bt], R.X. Yang [bm,ax], S.L. Yang [a,be], Y.H. Yang [al], Y.X. Yang [l], Yifan Yang [a,be], Zhi Yang [aa], M. Ye [a,ax], M.H. Ye [g], J.H. Yin [a], Z.Y. You [ay], B.X. Yu [a,ax,be], C.X. Yu [am], G. Yu [a,be], J.S. Yu [t,13], T. Yu [bn], C.Z. Yuan [a,be], W. Yuan [bp,br], X.Q. Yuan [an,12], Y. Yuan [a], Z.Y. Yuan [ay], C.X. Yue [ai], A. Yuncu [bb,1], A.A. Zafar [bo], Y. Zeng [t,13], B.X. Zhang [a], Guangyi Zhang [p], H.H. Zhang [ay], H.Y. Zhang [a,ax], J.L. Zhang [bu], J.Q. Zhang [d], J.W. Zhang [a,ax,be], J.Y. Zhang [a], J.Z. Zhang [a,be], Jianyu Zhang [a,be], Jiawei Zhang [a,be], L. Zhang [a], Lei Zhang [al], S. Zhang [ay], S.F. Zhang [al], T.J. Zhang [ar,8], X.Y. Zhang [aq], Y. Zhang [bk], Y.H. Zhang [a,ax], Y.T. Zhang [bm,ax], Yan Zhang [bm,ax], Yao Zhang [a], Yi Zhang [i,9], Z.H. Zhang [f], Z.Y. Zhang [bt], G. Zhao [a], J. Zhao [ai], J.Y. Zhao [a,be], J.Z. Zhao [a,ax], Lei Zhao [bm,ax], Ling Zhao [a], M.G. Zhao [am], Q. Zhao [a], S.J. Zhao [bw], Y.B. Zhao [a,ax], Y.X. Zhao [aa], Z.G. Zhao [bm,ax], A. Zhemchugov [ae,2], B. Zheng [bn], J.P. Zheng [a,ax], Y. Zheng [an,12], Y.H. Zheng [be], B. Zhong [ak], C. Zhong [bn], L.P. Zhou [a,be], Q. Zhou [a,be], X. Zhou [bt], X.K. Zhou [be], X.R. Zhou [bm,ax], A.N. Zhu [a,be], J. Zhu [am], K. Zhu [a], K.J. Zhu [a,ax,be], S.H. Zhu [bl], W.J. Zhu [am], X.L. Zhu [az], Y.C. Zhu [bm,ax], Z.A. Zhu [a,be], B.S. Zou [a], J.H. Zou [a]

[a] Institute of High Energy Physics, Beijing 100049, People's Republic of China
[b] Beihang University, Beijing 100191, People's Republic of China
[c] Beijing Institute of Petrochemical Technology, Beijing 102617, People's Republic of China
[d] Bochum Ruhr-University, D-44780 Bochum, Germany
[e] Carnegie Mellon University, Pittsburgh, PA 15213, USA

[f] Central China Normal University, Wuhan 430079, People's Republic of China
[g] China Center of Advanced Science and Technology, Beijing 100190, People's Republic of China
[h] COMSATS University Islamabad, Lahore Campus, Defence Road, Off Raiwind Road, 54000 Lahore, Pakistan
[i] Fudan University, Shanghai 200443, People's Republic of China
[j] G.I. Budker Institute of Nuclear Physics SB RAS (BINP), Novosibirsk 630090, Russia
[k] GSI Helmholtzcentre for Heavy Ion Research GmbH, D-64291 Darmstadt, Germany
[l] Guangxi Normal University, Guilin 541004, People's Republic of China
[m] Guangxi University, Nanning 530004, People's Republic of China
[n] Hangzhou Normal University, Hangzhou 310036, People's Republic of China
[o] Helmholtz Institute Mainz, Johann-Joachim-Becher-Weg 45, D-55099 Mainz, Germany
[p] Henan Normal University, Xinxiang 453007, People's Republic of China
[q] Henan University of Science and Technology, Luoyang 471003, People's Republic of China
[r] Huangshan College, Huangshan 245000, People's Republic of China
[s] Hunan Normal University, Changsha 410081, People's Republic of China
[t] Hunan University, Changsha 410082, People's Republic of China
[u] Indian Institute of Technology Madras, Chennai 600036, India
[v] Indiana University, Bloomington, IN 47405, USA
[w] INFN Laboratori Nazionali di Frascati, I-00044, Frascati, Italy
[x] INFN and University of Perugia, I-06100, Perugia, Italy
[y] INFN Sezione di Ferrara, I-44122, Ferrara, Italy
[z] University of Ferrara, I-44122, Ferrara, Italy
[aa] Institute of Modern Physics, Lanzhou 730000, People's Republic of China
[ab] Institute of Physics and Technology, Peace Ave. 54B, Ulaanbaatar 13330, Mongolia
[ac] Jilin University, Changchun 130012, People's Republic of China
[ad] Johannes Gutenberg University of Mainz, Johann-Joachim-Becher-Weg 45, D-55099 Mainz, Germany
[ae] Joint Institute for Nuclear Research, 141980 Dubna, Moscow region, Russia
[af] Justus-Liebig-Universitaet Giessen, II. Physikalisches Institut, Heinrich-Buff-Ring 16, D-35392 Giessen, Germany
[ag] KVI-CART, University of Groningen, NL-9747 AA Groningen, the Netherlands
[ah] Lanzhou University, Lanzhou 730000, People's Republic of China
[ai] Liaoning Normal University, Dalian 116029, People's Republic of China
[aj] Liaoning University, Shenyang 110036, People's Republic of China
[ak] Nanjing Normal University, Nanjing 210023, People's Republic of China
[al] Nanjing University, Nanjing 210093, People's Republic of China
[am] Nankai University, Tianjin 300071, People's Republic of China
[an] Peking University, Beijing 100871, People's Republic of China
[ao] Qufu Normal University, Qufu 273165, People's Republic of China
[ap] Shandong Normal University, Jinan 250014, People's Republic of China
[aq] Shandong University, Jinan 250100, People's Republic of China
[ar] Shanghai Jiao Tong University, Shanghai 200240, People's Republic of China
[as] Shanxi Normal University, Linfen 041004, People's Republic of China
[at] Shanxi University, Taiyuan 030006, People's Republic of China
[au] Sichuan University, Chengdu 610064, People's Republic of China
[av] Soochow University, Suzhou 215006, People's Republic of China
[aw] Southeast University, Nanjing 211100, People's Republic of China
[ax] State Key Laboratory of Particle Detection and Electronics, Beijing 100049, Hefei 230026, People's Republic of China
[ay] Sun Yat-Sen University, Guangzhou 510275, People's Republic of China
[az] Tsinghua University, Beijing 100084, People's Republic of China
[ba] Ankara University, 06100 Tandogan, Ankara, Turkey
[bb] Istanbul Bilgi University, 34060 Eyup, Istanbul, Turkey
[bc] Uludag University, 16059 Bursa, Turkey
[bd] Near East University, Nicosia, North Cyprus, Mersin 10, Turkey
[be] University of Chinese Academy of Sciences, Beijing 100049, People's Republic of China
[bf] University of Hawaii, Honolulu, HI 96822, USA
[bg] University of Jinan, Jinan 250022, People's Republic of China
[bh] University of Manchester, Oxford Road, Manchester, M13 9PL, United Kingdom
[bi] University of Minnesota, Minneapolis, MN 55455, USA
[bj] University of Muenster, Wilhelm-Klemm-Str. 9, 48149 Muenster, Germany
[bk] University of Oxford, Keble Rd, Oxford, OX13RH, United Kingdom
[bl] University of Science and Technology Liaoning, Anshan 114051, People's Republic of China
[bm] University of Science and Technology of China, Hefei 230026, People's Republic of China
[bn] University of South China, Hengyang 421001, People's Republic of China
[bo] University of the Punjab, Lahore, 54590, Pakistan
[bp] University of Turin, I-10125, Turin, Italy
[bq] University of Eastern Piedmont, I-15121, Alessandria, Italy
[br] INFN, I-10125, Turin, Italy
[bs] Uppsala University, Box 516, SE-75120 Uppsala, Sweden
[bt] Wuhan University, Wuhan 430072, People's Republic of China
[bu] Xinyang Normal University, Xinyang 464000, People's Republic of China
[bv] Zhejiang University, Hangzhou 310027, People's Republic of China
[bw] Zhengzhou University, Zhengzhou 450001, People's Republic of China

ARTICLE INFO

Article history:
Received 18 September 2020
Received in revised form 10 December 2020
Accepted 28 December 2020
Available online 6 January 2021
Editor: L. Rolandi

ABSTRACT

Born cross sections for the processes $e^+e^- \to \omega\eta$ and $e^+e^- \to \omega\pi^0$ have been determined for center-of-mass energies between 2.00 and 3.08 GeV with the BESIII detector at the BEPCII collider. The results obtained in this work are consistent with previous measurements but with improved precision. Two resonant structures are observed. In the $e^+e^- \to \omega\eta$ cross sections, a resonance with a mass of $(2176 \pm 24 \pm 3)\,\mathrm{MeV}/c^2$ and a width of $(89 \pm 50 \pm 5)\,\mathrm{MeV}$ is observed with a significance of 6.2σ. Its properties

Keywords:
BESIII
$\phi(2170)$
Excited ω states
Excited ρ states

are consistent with the $\phi(2170)$. In the $e^+e^- \to \omega\pi^0$ cross sections, a resonance denoted $Y(2040)$ is observed with a significance of more than 10σ. Its mass and width are determined to be $(2034 \pm 13 \pm 9)\,\mathrm{MeV}/c^2$ and $(234 \pm 30 \pm 25)\,\mathrm{MeV}$, respectively, where the first uncertainties are statistical and the second ones are systematic.

1. Introduction

In low-energy e^+e^- collision experiments, the vector mesons ρ, ω, and ϕ and their low lying excited states can be produced abundantly. The Particle Data Group (PDG) [1] has tabulated experimental results for these states. However, some of the higher lying excitations are not fully identified yet. It is especially in the region around 2 GeV where further experimental insight is needed to resolve the situation involving resonances such as the $\rho(2000)$, $\rho(2150)$ and $\phi(2170)$ states.

Considerable efforts have been made theoretically to understand the nature of the $\phi(2170)$ resonance, and several interpretations have been proposed, such as an $s\bar{s}g$ hybrid [2,3], an $s\bar{s}$ meson [4–7], an $s\bar{s}s\bar{s}$ tetraquark state [8–13], a $\Lambda\bar{\Lambda}$ bound state [14–16], as well as $\phi K\bar{K}$ [17] and $\phi f_0(980)$ [18] resonances. These models differ in their predictions of the branching fractions of the $\phi(2170)$ to decay channels such as $\phi\eta$ or $K^{(*)}\bar{K}^{(*)}$ as certain decay modes can either be suppressed or favored depending on its nature [2,4,19–21]. It is therefore of great importance to measure the branching fractions for a variety of different decay channels in order to help in discriminating between different models.

The $\phi(2170)$ state was first observed by the BaBar experiment in the initial state radiation (ISR) process $e^+e^- \to \gamma_{\rm ISR}\phi f_0(980)$ [22] and later confirmed by the BESII and BESIII experiments in $J/\psi \to \eta\phi f_0(980)$ [23,24] as well as by both the BaBar and Belle experiments in the aforementioned ISR process [25,26]. The observed masses and widths of the $\phi(2170)$ range from $(2079 \pm 13^{+79}_{-28})\,\mathrm{MeV}/c^2$ [26] to $(2200 \pm 6 \pm 5)\,\mathrm{MeV}/c^2$ [24] and $(58 \pm 16 \pm 20)\,\mathrm{MeV}$ [22] to $(192 \pm 23^{+25}_{-61})\,\mathrm{MeV}$ [25], respectively.

Several studies of the properties of the $\phi(2170)$ resonance have recently been made by the BESIII experiment. A partial-wave analysis was performed for the $e^+e^- \to K^+K^-\pi^0\pi^0$ process [27], in which indications for sizable partial widths of the $\phi(2170)$ resonance to the $K^+(1460)K^-$, $K_1^+(1270)K^-$ and $K_1^+(1400)K^-$ channels (here, charge-conjugation is implied) were found. Attempts were also made to study channels with simpler topologies, including $e^+e^- \to K^+K^-$, where a resonance with mass $(2239.2 \pm 7.1 \pm 11.3)\,\mathrm{MeV}/c^2$ and width $(139.8 \pm 12.3 \pm 20.6)\,\mathrm{MeV}$ was found [28,29], and $e^+e^- \to \phi\eta'$ [30], where a resonance with mass $(2177.5 \pm 5.1 \pm 18.6)\,\mathrm{MeV}/c^2$ and width $(149.0 \pm 15.6 \pm 8.9)\,\mathrm{MeV}$ was found. In $e^+e^- \to \phi K^+K^-$, a sharp enhancement is observed in the Born cross section at $\sqrt{s} = 2.2324$ GeV, which is close to the mass of the $\phi(2170)$ resonance [31], however its width seems to be incompatible with that of the $\phi(2170)$.

A comparison of decay channels without hidden or open strangeness such as $e^+e^- \to \omega\eta$ to those observed thus far can provide additional information about the properties of the $\phi(2170)$ resonance. In addition, this process can also be used to study excited ω resonances appearing as $\omega^* \to \omega\eta$ [32], which is expected to be one of the dominant decay channels for excited ω mesons and a benchmark process to study their properties.

In contrast to the $e^+e^- \to \omega\eta$ process, the reaction $e^+e^- \to \omega\pi^0$ allows the study of the isovector vector mesons and their excited states. Generally, the excited ρ states around 2 GeV/c^2 are not well understood. Although there are two results on the so-called $\rho(2000)$ [33,34], its existence is not well-established. Furthermore, several experiments have claimed the observation of the $\rho(2150)$ state with mass and width lying in the range of 1.990 to $2.254\,\mathrm{GeV}/c^2$ and 70 to 389 MeV, respectively [35–39].

In an approach based on the quark-pair-creation model, the $\rho(2150)$ state is identified as a candidate for the 4^3S_1 state [40,41]. The Born cross section of $e^+e^- \to \omega\pi^0$ in the energy region below 2 GeV has been measured by several experiments [42–49], while the data above 2 GeV is rather scarce. Thus, more measurements of $e^+e^- \to \omega\pi^0$ above 2 GeV are of high interest to study the properties of excited ρ states.

In this letter, we present Born cross section measurements of the processes $e^+e^- \to \omega\eta$ and $e^+e^- \to \omega\pi^0$ with subsequent $\omega \to \pi^+\pi^-\pi^0$, $\pi^0 \to \gamma\gamma$ and $\eta \to \gamma\gamma$ decays.

2. Detector and data sample

The BESIII detector is a magnetic spectrometer [50] located at the Beijing Electron Position Collider (BEPCII) [51]. The cylindrical core of the BESIII detector consists of a helium-based multilayer drift chamber (MDC), a plastic scintillator time-of-flight system (TOF), and a CsI(Tl) electromagnetic calorimeter (EMC), which are all enclosed in a superconducting solenoidal magnet providing a 1.0 T magnetic field. The solenoid is supported by an octagonal flux-return yoke with resistive plate counter muon identifier modules interleaved with steel. The acceptance of charged particles and photons is 93% over 4π solid angle. The charged-particle momentum resolution at 1 GeV/c is 0.5%, and the dE/dx resolution is 6% for the electrons from Bhabha scattering. The EMC measures photon energies with a resolution of 2.5% (5%) at 1 GeV in the barrel (end cap) region. The time resolution of the TOF barrel part is 68 ps, while that of the end cap part is 110 ps.

The data samples used in this letter have been collected with the BESIII detector at 22 center-of-mass (c.m.) energies from 2.000 to 3.080 GeV, corresponding to a total integrated luminosity of 651 pb^{-1}.

The GEANT4 based [52] simulation software BOOST [53] is used to produce Monte Carlo (MC) simulation samples. Events are generated using the ConExc generator [54] with ISR and vacuum polarization (VP) taken into account. Inclusive hadron production of the type $e^+e^- \to$ hadrons is simulated to estimate possible background processes and to optimize event selection criteria. Exclusive MC samples are generated to determine the detection efficiencies of the signal processes. Since the beam energy spread of BEPCII is less than 1 MeV at $\sqrt{s} < 3$ GeV, it is much smaller than the experimental resolution of the BESIII detector and can thus be ignored in the simulation.

3. Event selection and determination of the Born cross section

3.1. Analysis of $e^+e^- \to \omega\eta$

For $e^+e^- \to \omega\eta$ (with subsequent $\omega \to \pi^+\pi^-\pi^0$, $\pi^0 \to \gamma\gamma$ and $\eta \to \gamma\gamma$ decays), candidate events are required to have at least two reconstructed charged tracks and at least four reconstructed photons. Each charged track is required to be located within the MDC acceptance, $|\cos\theta| < 0.93$, where θ is the polar angle of the charged track, and to originate from a cylinder around the interaction point of 1 cm radius and extending ± 10 cm

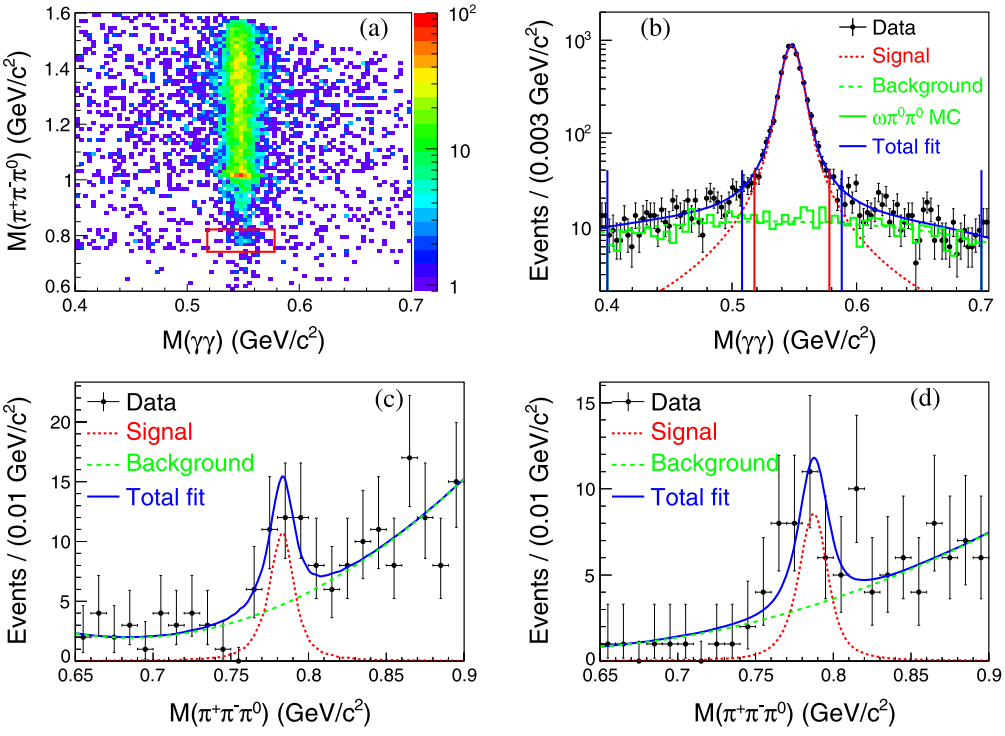

Fig. 1. Invariant mass distributions for data taken at $\sqrt{s} = 2.125$ GeV. (a) Distribution of the $\pi^+\pi^-\pi^0$ invariant mass versus the two-photon invariant mass. The area marked in red corresponds to the signal region. (b) Fit to the $M(\gamma\gamma)$ distribution, where the (black) dots with error bars are data, the (blue) solid curve is the total fit result, the (green) dashed curve indicates background described by a second order Chebychev polynomial, the (red) dotted curve is the $\eta \to \gamma\gamma$ signal shape described by a Voigt function and the (green) histogram is the $e^+e^- \to \omega\pi^0\pi^0$ MC sample scaled to the integral of the background function in the fit. The vertical lines indicate the signal (red) and sideband regions (blue). (c) and (d) represent the $M(\pi^+\pi^-\pi^0)$ invariant mass distributions in the η signal and sideband region, respectively. The dots with error bars are data, the solid curves are the total fit results, the dashed curves indicate the background described by a second order Chebychev polynomial and the dotted curves are the ω signal shapes determined from MC simulations convolved with a Gaussian accounting for a potential difference in resolution between data and MC simulation.

along the detector axis. Information from TOF and dE/dx measurements is combined to form particle identification (PID) likelihoods for the π, K, and p hypotheses. Each track is assigned a particle type corresponding to the hypothesis with the highest PID likelihood. Exactly two oppositely charged pions are required in each event. Photon candidates are reconstructed using clusters of energy deposited in the EMC crystals. The energy is required to be larger than 25 MeV in the barrel region ($|\cos\theta| < 0.80$) and larger than 50 MeV in the end cap region ($0.86 < |\cos\theta| < 0.92$). The energy deposited in nearby TOF counters is included to improve the reconstruction efficiency and energy resolution. The difference of the EMC time from the event start time is required to be within [0,700] ns to suppress electronic noise and showers unrelated to the event.

To improve the momentum and energy resolution and to suppress background events, a four-constraint (4C) kinematic fit imposing four-momentum conservation is performed under the hypothesis $e^+e^- \to \pi^+\pi^-4\gamma$. For the goodness of the kinematic fit, $\chi^2_{\rm 4C} < 70$ is required. For events with more than four photon candidates, the combination with the smallest $\chi^2_{\rm 4C}$ is retained. In addition, a kinematic fit for the alternative hypothesis $e^+e^- \to \pi^+\pi^-5\gamma$ is performed and only those events that satisfy $\chi^2_{\rm 4C}(\pi^+\,\pi^-4\gamma) < \chi^2_{\rm 4C}(\pi^+\pi^-5\gamma)$ are retained in order to suppress backgrounds from $e^+e^- \to \omega\pi^0\pi^0$ events. Two photon pairs corresponding to the best $\pi^0\eta$, $\pi^0\pi^0$ and $\eta\eta$ candidates are selected separately by choosing the combination with the smallest value of $\chi^2_{\alpha\beta} = (M(\gamma_1\gamma_2) - m_\alpha)^2/\sigma^2_{12} + (M(\gamma_3\gamma_4) - m^2_\beta)/\sigma^2_{34}$, where α and β represent either π^0 or η, and the mass resolution $\sigma_{12(34)}$ in the invariant mass region of the π^0 or η meson is obtained from MC simulations. Only combinations with $\chi^2_{\pi^0\eta} < \chi^2_{\pi^0\pi^0}$ and $\chi^2_{\pi^0\eta} < \chi^2_{\eta\eta}$ are retained. The π^0 and η candidates are selected by requiring $|M(\gamma_1\gamma_2) - m_{\pi^0}| < 0.02\,{\rm GeV}/c^2$ and $|M(\gamma_3\gamma_4) - m_\eta| < 0.03\,{\rm GeV}/c^2$, corresponding to about 3σ intervals around the respective nominal masses of π^0 and η, m_{π^0} and m_η [1]. Events with $|E_{\gamma_3} - E_{\gamma_4}|/p_\eta > 0.9$, where p_η is the momentum of the η meson in the laboratory system, are rejected to suppress background events from the $e^+e^- \to \omega\gamma_{\rm ISR}$ and $e^+e^- \to \omega\pi^0\pi^0$ processes.

The distribution of the $\pi^+\pi^-\pi^0$ invariant mass versus the two-photon invariant mass of the selected events at $\sqrt{s} = 2.125$ GeV is shown as an example in Fig. 1(a), where an ω signal around the nominal ω meson mass is visible. Potential background reactions to the $e^+e^- \to \omega\eta$ process are studied using both inclusive e^+e^- → hadrons and exclusive MC samples. Simulated events are subject to the same selection procedure as that applied to the experimental data. According to MC simulations, the dominant background stems from $e^+e^- \to \pi^+\pi^-\pi^0\eta$, which contains the same final state particles as the signal reaction. The $e^+e^- \to \omega\pi^0\pi^0$ and $e^+e^- \to \omega\gamma_{\rm ISR}$ processes form a peaking background contribution in the $\pi^+\pi^-\pi^0$ invariant mass distribution. The total peaking background from $e^+e^- \to \omega\gamma_{\rm ISR}$ is estimated by MC simulations normalized to the experimental luminosity and is found to be negligible. The peaking background from $e^+e^- \to \omega\pi^0\pi^0$ is inferred from the η sidebands, which are defined as $0.400 < M(\gamma_3\gamma_4) < 0.508\,{\rm GeV}/c^2$ and $0.588 < M(\gamma_3\gamma_4) < 0.700\,{\rm GeV}/c^2$ as shown in Fig. 1(b).

To determine the signal yield of the $e^+e^- \to \omega\eta$ process, a simultaneous unbinned maximum likelihood fit is performed to the $M(\pi^+\pi^-\pi^0)$ spectra in both the η signal and sideband regions at each energy, where the shapes of signal and background are shared. Fig. 1 (c) and (d) show the fit results in signal and sideband regions at 2.125 GeV. The signal is modeled with the peak shape obtained from MC simulation convolved with a Gaussian function allowing for a potential resolution difference between data

Table 1
The Born cross sections of the $e^+e^- \to \omega\eta$ process. In addition, upper limits are given at 90% confidence level. All symbols defined are the same as those in Eq. (1). In the column of Born cross section σ, the first uncertainty is statistical, and the second one is systematic. Sig. is the significance of the observed signal. VP lists the vacuum polarization factor.

$\sqrt{s}$ (GeV)	$N_{\rm sig}$	$N_{\rm sig}^{\rm up}$	$\mathcal{L}$ (pb^{-1})	$\varepsilon\cdot(1+\delta)$	σ (pb)	$\sigma^{\rm up}$ (pb)	Sig. (σ)	VP
2.0000	$19.3^{+5.9}_{-5.2}$	<27.3	10.1	0.158	$34.7^{+10.6}_{-9.3}\pm2.9$	<49.3	4.5	1.037
2.0500	$2.3^{+2.6}_{-1.9}$	<7.0	3.34	0.161	$12.6^{+13.7}_{-10.1}\pm1.0$	<37.5	1.4	1.038
2.1000	$1.9^{+3.8}_{-1.9}$	<8.2	12.2	0.162	$2.8^{+5.6}_{-2.8}\pm0.2$	<11.9	0.5	1.039
2.1250	$17.2^{+8.2}_{-7.5}$	<26.0	108	0.163	$2.8^{+1.3}_{-1.2}\pm0.3$	<4.3	2.2	1.039
2.1500	$2.3^{+2.3}_{-1.6}$	<6.0	2.84	0.151	$15.6^{+15.7}_{-11.0}\pm0.7$	<40.3	1.1	1.040
2.1750	$9.2^{+4.1}_{-3.4}$	<14.9	10.6	0.156	$16.0^{+7.1}_{-6.0}\pm1.0$	<25.9	3.0	1.040
2.2000	$16.5^{+5.5}_{-4.8}$	<25.0	13.7	0.153	$22.7^{+7.5}_{-6.5}\pm1.7$	<34.3	4.3	1.040
2.2324	$22.9^{+5.8}_{-5.1}$	<30.9	11.9	0.161	$34.4^{+8.7}_{-7.7}\pm2.2$	<46.4	>5	1.041
2.3094	$11.9^{+5.3}_{-4.6}$	<22.6	21.1	0.178	$9.1^{+4.1}_{-3.5}\pm0.7$	<17.3	3.7	1.041
2.3864	$8.2^{+3.9}_{-3.3}$	<14.5	22.5	0.173	$6.1^{+2.9}_{-2.4}\pm0.4$	<10.7	2.6	1.041
2.3960	$20.6^{+6.3}_{-5.6}$	<29.6	66.9	0.172	$5.2^{+1.6}_{-1.4}\pm0.4$	<7.4	3.5	1.041
2.5000	$2.6^{+2.4}_{-1.7}$	<6.3	1.10	0.175	$39.3^{+35.7}_{-25.0}\pm3.5$	<94.2	1.6	1.041
2.6444	$17.7^{+5.2}_{-4.5}$	<23.3	33.7	0.174	$8.7^{+2.6}_{-2.2}\pm0.5$	<11.4	>5	1.039
2.6464	$18.8^{+5.1}_{-4.4}$	<26.0	34.0	0.173	$9.2^{+2.5}_{-2.2}\pm0.6$	<12.7	>5	1.039
2.7000	$1.2^{+1.9}_{-1.0}$	<2.2	1.03	0.177	$19.6^{+29.3}_{-15.2}\pm0.9$	<34.7	1.1	1.039
2.8000	$1.2^{+1.9}_{-1.0}$	<2.2	1.01	0.177	$20.0^{+29.8}_{-15.5}\pm0.9$	<35.4	1.1	1.037
2.9000	$27.0^{+6.0}_{-5.3}$	<30.3	105	0.182	$4.1^{+0.9}_{-0.8}\pm0.3$	<4.6	>5	1.033
2.9500	$1.8^{+2.1}_{-1.8}$	<5.0	15.9	0.184	$1.8^{+2.1}_{-1.7}\pm0.1$	<4.9	0.7	1.029
2.9810	$0.7^{+1.8}_{-0.7}$	<4.4	16.1	0.187	$0.7^{+1.8}_{-0.7}\pm0.1$	<4.2	0.2	1.025
3.0000	$0.0^{+0.5}_{-0.0}$	<2.2	15.9	0.186	$0.0^{+0.5}_{-0.0}\pm0.0$	<2.1	0.0	1.021
3.0200	$0.3^{+1.4}_{-0.3}$	<2.2	17.3	0.184	$0.3^{+1.3}_{-0.3}\pm0.0$	<2.0	0.3	1.014
3.0800	$9.2^{+4.5}_{-3.8}$	<15.8	126	0.172	$1.2^{+0.6}_{-0.5}\pm0.1$	<2.1	2.8	0.915

and MC simulation. The background is described with a second-order Chebychev polynomial. In the fit, peaking background is automatically subtracted by constructing the number of ω events in the η signal region as $N_{\rm obs} = N_{\rm sig} + f_{\rm scale}\cdot N_{\rm bkg}$, where $N_{\rm sig}$ is the number of $\omega\eta$ signal events, $N_{\rm bkg}$ is the number of ω events in the η sideband region, and $f_{\rm scale}$ is the normalization factor $f_{\rm scale} = N^{\eta_{\rm sig}}/N^{\eta_{\rm sideband}}$ where $N^{\eta_{\rm sig}}(N^{\eta_{\rm sideband}})$ is the number of background events falling into the signal (sideband) region as shown in Fig. 1(b).

The Born cross section of the $e^+e^- \to \omega\eta$ process is calculated according to

$$\sigma = \frac{N_{\rm sig}}{\mathcal{L}\cdot\varepsilon\cdot(1+\delta)\cdot\mathcal{B}}, \quad (1)$$

where $\mathcal{L}$ is the integrated luminosity of the individual dataset, $(1+\delta)$ is the radiative correction factor accounting for both ISR and VP, and ε is the product of geometrical acceptance and selection efficiency obtained from MC simulation. The total branching fraction $\mathcal{B}$ is the product of the branching fractions for the decays contained in the full decay chain $\mathcal{B} = \mathcal{B}(\omega\to\pi^+\pi^-\pi^0)\cdot\mathcal{B}(\pi^0\to\gamma\gamma)\cdot\mathcal{B}(\eta\to\gamma\gamma) = 34.7\%$. The Born cross sections as well as upper limits at the 90% confidence level are given for all 22 energy points together with all values used in the calculation in Table 1. VP factors are also listed for the convenience of calculating dressed cross sections. The results are consistent with previous measurements [55–57] but with improved precision. A comparison to the previous results is shown in Fig. 2(a).

Various sources of systematic uncertainties concerning the measurement of the Born cross sections are investigated, including integrated luminosity, branching fractions, ISR and VP correction factors, event selection criteria, the fit procedure of the signal, and the contributions from peaking background processes.

The integrated luminosity at each energy point is measured using large angle Bhabha events with an uncertainty of 1% following the method in Ref. [58]. The uncertainties associated with the branching fractions of intermediate states are taken from the PDG [1]. The uncertainty of the ISR and VP correction factors is obtained from the accuracy of radiation function, which is about 0.5% [54], and has an additional contribution from the cross section lineshape, which is estimated by varying the model parameters of the fit to the cross sections. All parameters are randomly varied within their uncertainties and the resulting parametrization of the lineshape is used to recalculate $(1+\delta)$, ε and the corresponding cross sections. This procedure is repeated 1000 times and the standard deviation of the resulting cross sections is taken as a systematic uncertainty. Differences between the data and MC simulation for the tracking efficiency and PID of charged pions are investigated using the high-purity control sample of $e^+e^-\to K^+K^-\pi^+\pi^-$ [28,59]. The photon detection efficiency is studied with a sample of $e^+e^-\to K^+K^-\pi^+\pi^-\pi^0$ with similar method for tracking uncertainty [59]. The result shows that the difference in detection efficiency between data and MC simulation is 1% per photon. The uncertainties associated with the kinematic fit are studied with the track helix parameter correction method, as described in Ref. [60].

Due to the limited statistics in the data samples, a control sample of the $J/\psi\to\omega\eta$ decay is used to estimate the uncertainties arising from the selection conditions $\chi^2_{\rm 4C}(\pi^+\pi^-4\gamma) < \chi^2_{\rm 4C}(\pi^+\pi^-5\gamma)$, $\chi^2_{\pi^0\eta} < \chi^2_{\pi^0\pi^0}$, $\chi^2_{\pi^0\eta} < \chi^2_{\eta\eta}$, $|M(\gamma_1\gamma_2) - m_{\pi^0}| < 0.02\,{\rm GeV}/c^2$, $|M(\gamma_3\gamma_4) - m_\eta| < 0.03\,{\rm GeV}/c^2$ and $|E_{\gamma_3} - E_{\gamma_4}|/p_\eta < 0.9$. For this, the single-requirement efficiency is studied, removing one of the selection conditions at a time and studying the change in the number of observed events. In case a significant difference is found between the data control sample and a MC simulation of the $J/\psi\to\omega\eta$ decay, this difference is taken as the systematic uncertainty.

Due to large statistical fluctuations in the data, toy MC samples are used to estimate the systematic uncertainties stemming from the description of the signal and background shape as well as from

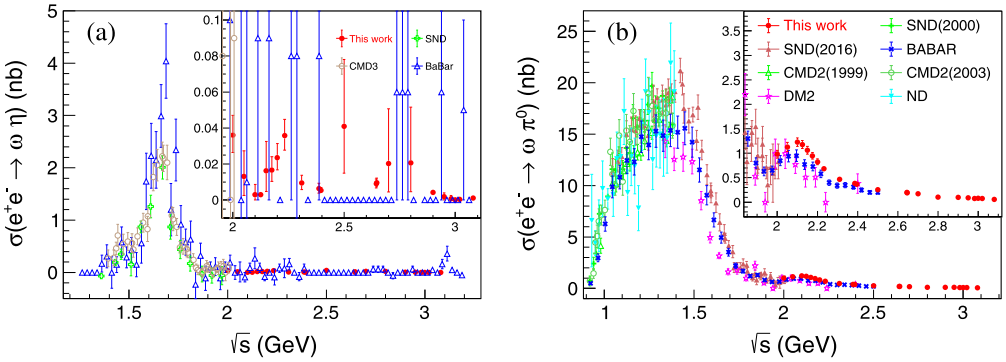

Fig. 2. Dressed cross sections for the processes (a) $e^+e^- \to \omega\eta$ and (b) $e^+e^- \to \omega\pi^0$. In comparison to the data presented in this work (red dots), in (a) the data from the CMD3 [56] (brown open circles), SND [55] (green open crosses) and BaBar [57] (blue open triangles) experiments are shown. In (b), our data is compared to the results of the CMD2 [46,47] (green open upward triangles and green open circles), SND [42,44] (green filled crosses and brown filled triangles), BaBar [49] (blue filled X crosses), DM2 [48] (magenta open stars) and ND [45] (cyan filled downward triangles) experiments.

Table 2
Summary of relative systematic uncertainties (in %) associated with the luminosity ($\mathcal{L}$), the tracking efficiency (Track), the photon detection efficiency (Photon), PID, Branching fraction (Br), χ^2 requirement, 4C kinematic fit (4C), $|E_{\gamma_3} - E_{\gamma_4}|/p_\eta < 0.9$ (Angle), background shape (Bkg), signal shape (Sig), fit range (Range), η and π^0 mass windows (m(η) and m(π^0)), peaking background (Peak), the initial state radiation and the vacuum polarization correction factor $(1+\delta)$ in the measurement of the Born cross section of the $e^+e^- \to \omega\eta$ process.

Energies	$\mathcal{L}$	Track	Photon	PID	Br	χ^2	4C	Angle	Bkg	Sig	Range	m(η)	m(π^0)	Peak	$1+\delta$	Total
2.0000	1.0	2.0	4.0	2.0	0.9	0.5	0.6	1.1	0.1	2.5	0.2	0.4	3.0	4.8	0.5	8.1
2.0500	1.0	2.0	4.0	2.0	0.9	0.5	0.6	1.1	0.1	2.5	0.2	0.4	3.0	4.8	0.6	8.2
2.1000	1.0	2.0	4.0	2.0	0.9	0.5	0.6	1.1	1.9	2.5	2.2	0.4	3.0	9.6	2.7	12
2.1250	1.0	2.0	4.0	2.0	0.9	0.5	0.5	1.1	1.9	2.5	2.2	0.4	3.0	9.6	1.1	12
2.1500	1.0	2.0	4.0	2.0	0.9	0.5	0.6	1.1	0.5	2.5	0.5	0.4	3.0	3.7	1.5	7.7
2.1750	1.0	2.0	4.0	2.0	0.9	0.5	0.7	1.1	0.5	2.5	0.5	0.4	3.0	3.7	1.2	7.7
2.2000	1.0	2.0	4.0	2.0	0.9	0.5	0.5	1.1	0.3	1.6	0.2	0.4	3.0	2.6	1.8	7.0
2.2324	1.0	2.0	4.0	2.0	0.9	0.5	0.7	1.1	0.2	0.8	0.7	0.4	3.0	1.6	1.5	6.5
2.3094	1.0	2.0	4.0	2.0	0.9	0.5	0.7	1.1	0.1	2.0	0.1	0.4	3.0	2.1	0.7	6.8
2.3864	1.0	2.0	4.0	2.0	0.9	0.5	0.6	1.1	1.0	1.6	1.2	0.4	3.0	2.3	0.5	6.9
2.3960	1.0	2.0	4.0	2.0	0.9	0.5	0.5	1.1	0.1	2.2	0.2	0.4	3.0	2.6	0.5	7.0
2.5000	1.0	2.0	4.0	2.0	0.9	0.5	0.6	1.1	0.1	2.2	0.2	0.4	3.0	2.6	0.5	7.0
2.6444	1.0	2.0	4.0	2.0	0.9	0.5	0.6	1.1	0.2	1.4	0.6	0.4	3.0	1.6	0.5	6.5
2.6464	1.0	2.0	4.0	2.0	0.9	0.5	0.6	1.1	0.1	0.8	0.8	0.4	3.0	1.7	0.5	6.4
2.7000	1.0	2.0	4.0	2.0	0.9	0.5	0.6	1.1	0.1	0.8	0.8	0.4	3.0	1.7	0.5	6.4
2.8000	1.0	2.0	4.0	2.0	0.9	0.5	0.6	1.1	0.1	0.8	0.8	0.4	3.0	1.7	0.5	6.4
2.9000	1.0	2.0	4.0	2.0	0.9	0.5	0.5	1.1	0.2	0.4	0.8	0.4	3.0	1.7	0.5	6.4
2.9500	1.0	2.0	4.0	2.0	0.9	0.5	0.6	1.1	0.2	0.4	0.8	0.4	3.0	1.7	0.5	6.4
2.9810	1.0	2.0	4.0	2.0	0.9	0.5	0.6	1.1	0.2	0.4	0.8	0.4	3.0	1.7	0.5	6.4
3.0000	1.0	2.0	4.0	2.0	0.9	0.5	0.6	1.1	0.2	0.4	0.8	0.4	3.0	1.7	0.5	6.4
3.0200	1.0	2.0	4.0	2.0	0.9	0.5	0.6	1.1	0.2	0.4	0.8	0.4	3.0	1.7	0.5	6.4
3.0800	1.0	2.0	4.0	2.0	0.9	0.5	0.7	1.1	0.4	1.6	0.9	0.4	3.0	2.7	0.5	6.9

the fit range when determining $N_{\rm obs}$. A total of 500 sets of toy MC samples are generated according to the final fit result shown in Fig. 1(c) with the same statistics as in data. For each toy MC sample, the following procedure is performed: the ω signal shape is changed to a Breit-Wigner function convolved with a Gaussian, the background shape is varied from a second to a third order Chebychev polynomial and the fit range is varied by $\pm 10\,{\rm MeV}/c^2$. The mean value of the differences of the signal yield between the nominal and the alternative fits is taken as the systematic uncertainty. The uncertainty of peaking background is related to the uncertainty of $N_{\rm bkg}$ and $f_{\rm scale}$. We estimate uncertainty of $N_{\rm bkg}$ with the same method for $N_{\rm obs}$, and that of $f_{\rm scale}$ by considering the fit uncertainty of the non-η background at 2.125 GeV. Since the statistics are quite low at several energy points, the uncertainties related to the fit of peaking background and the signal are quoted from nearby energy points when the signal significance is lower than 2σ.

The total systematic uncertainty for the Born cross section measurement is determined to be 12% for the $e^+e^- \to \omega\eta$ process at $\sqrt{s} = 2.125$ GeV. The uncertainties at the other c.m. energies are determined accordingly and are summarized in Table 2.

3.2. Analysis of $e^+e^- \to \omega\pi^0$

The event selection criteria for the $e^+e^- \to \omega\pi^0$ process are mostly the same as described in Sec. 3.1. The $\pi^0\pi^0$ candidate pairs are selected by minimizing $\chi^2_{\pi^0\pi^0} = (M(\gamma_1\gamma_2) - m_{\pi^0})^2/\sigma^2_{12} + (M(\gamma_3\gamma_4) - m_{\pi^0})^2/\sigma^2_{34}$. These π^0 candidates are required to be in a mass window of $(m_{\pi^0} - 0.02\,{\rm GeV}/c^2, m_{\pi^0} + 0.02\,{\rm GeV}/c^2)$. Since there are two π^0 candidates, the $\pi^+\pi^-\pi^0$ combination whose invariant mass is closest to m_ω is retained as the ω candidate, where the π^0 is denoted as π^0_ω to distinguish it from the bachelor pion $\pi^0_{\rm bach}$.

Using the above selection criteria, the distribution of the invariant mass of $\pi^+\pi^-\pi^0_\omega$ versus the two-photon invariant mass for $\pi^0_{\rm bach}$ candidates is depicted in Fig. 3(a). The ω signal is clearly evident.

A method similar to that described in Sec. 3.1 is used to study possible background contributions. According to the study, the dominant background stems from the four body process $e^+e^- \to \pi^+\pi^-\pi^0\pi^0$, which has the same final state particles as the signal channel. In a similar way as in the $e^+e^- \to \omega\eta$ case, possible peaking background contributions are inferred from the $\pi^0_{\rm bach}$ sideband regions defined as $0.055 < |M(\gamma_1\gamma_2) - m_{\pi^0}| < 0.095\,{\rm GeV}/c^2$

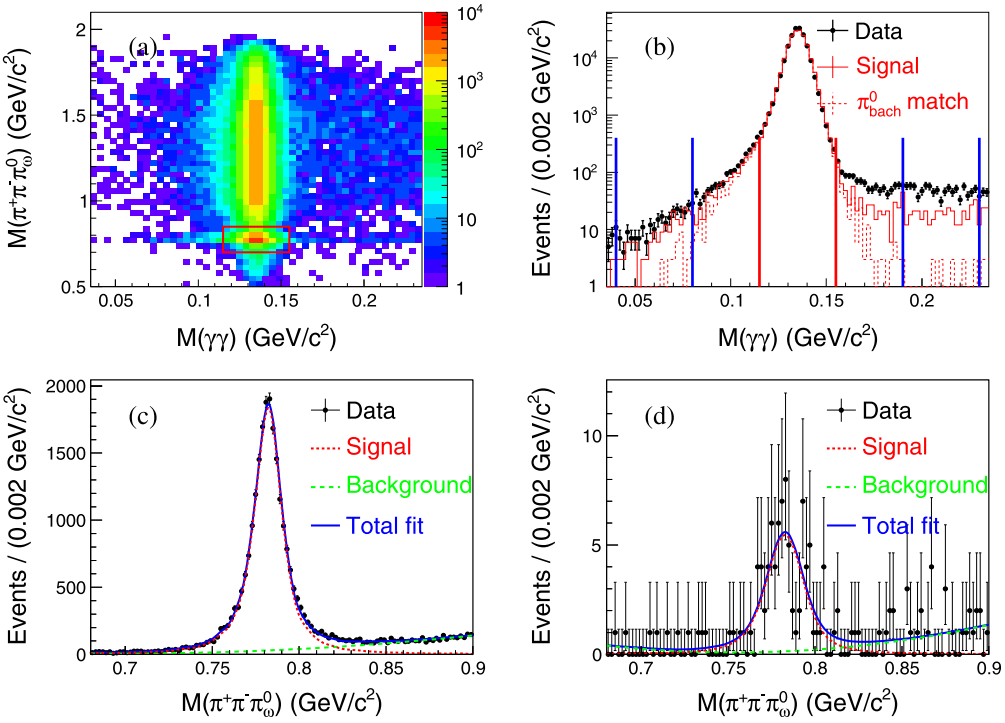

Fig. 3. Invariant mass distributions at $\sqrt{s} = 2.125$ GeV. (a) Distribution of the $\pi^+\pi^-\pi^0_\omega$ invariant mass versus the two-photon invariant mass corresponding to the $\pi^0_{\rm bach} \to \gamma\gamma$ decay. The red box indicates the signal region. (b) Distribution of the two-photon invariant mass $M(\gamma\gamma)$ corresponding to the $\pi^0_{\rm bach} \to \gamma\gamma$ decay, where the (black) dots with error bars are data, the (red) solid histogram and the (red) dashed histogram is the signal MC before and after $\pi^0_{\rm bach}$ matching with the MC truth information. The red and blue vertical lines indicate the signal and sideband regions, respectively. (c) and (d) represent the $M(\pi^+\pi^-\pi^0_\omega)$ distribution corresponding to $\pi^0_{\rm bach}$ signal and sideband regions, respectively. The (black) dots with error bars are data, the (blue) solid curves are the total fit results, the (green) dashed curves indicate the background contributions described by a second order Chebychev polynomial and the (red) dotted curves show the ω signal shapes described by the MC lineshape convolved with a Gaussian function.

(as illustrated in Fig. 3(b)). Note that due to mis-combination of photons, a large fraction of the π^0 sideband is composed of signal reactions. Still, while a peaking sideband contribution is found, its fraction is negligible (and would still have to be scaled down in a similar procedure as described for the $\omega\eta$ process) compared to the signal region as shown in Fig. 3 (c) and (d).

The signal yield is determined using the $M(\pi^+\pi^-\pi^0_\omega)$ mass spectra (as shown in Fig. 3(c)) with a similar method as described in Sec. 3.1, with the difference being that peaking backgrounds are neglected, so that the fit reduces to a one-dimensional unbinned likelihood fit. The fit yields $N_{\rm sig} = 22627 \pm 180$ events.

The Born cross section of the $e^+e^- \to \omega\pi^0$ process is calculated using Eq. (1), with the product of the branching fractions determined by $\mathcal{B} = \mathcal{B}(\omega \to \pi^+\pi^-\pi^0) \cdot \mathcal{B}^2(\pi^0 \to \gamma\gamma) = 87.1\%$. The values used in the calculation of the Born cross section of the $e^+e^- \to \omega\pi^0$ process are listed in Table 3, together with the results at all c.m. energies. The results are consistent with most of the previous measurements [42–48] but with improved precision, however, there exists a small difference with the BaBar measurement [49] at center-of-mass energies around 2.1 GeV. A comparison is shown in Fig. 2(b).

Concerning the systematic uncertainties, the contribution stemming from the luminosity determination is common for the $e^+e^- \to \omega\eta$ and $e^+e^- \to \omega\pi^0$ reactions. Furthermore, for the uncertainties relating to the detection efficiencies, the radiative corrections, the fitting procedure and the branching fractions taken from the literature, the same method is applied as previously stated in Sec. 3.1. In addition, the uncertainty arising from the π^0 selection is obtained by varying the mass window requirements for both π^0_ω and $\pi^0_{\rm bach}$ and examining the changes in the resulting cross sections. The total systematic uncertainty of the determination of the Born cross section is determined to be 6.7% for $e^+e^- \to \omega\pi^0$ at $\sqrt{s} = 2.125$ GeV. The uncertainties at the other c.m. energies are determined accordingly and are summarized in Table 4.

Table 3
The Born cross sections of the $e^+e^- \to \omega\pi^0$ process. The symbols are the same as those in Eq. (1). In the column of the Born cross section σ, the first uncertainty is statistical and the second one is systematic.

$\sqrt{s}$ (GeV)	$N_{\rm sig}$	$\mathcal{L}$ (pb^{-1})	$\varepsilon \cdot (1+\delta)$	σ (pb)
2.0000	1677 ± 50	10.1	0.202	946 ± 28 ± 70
2.0500	652 ± 31	3.34	0.205	1086 ± 52 ± 73
2.1000	2614 ± 62	12.2	0.209	1181 ± 28 ± 80
2.1250	22627 ± 180	108	0.211	1136 ± 9 ± 76
2.1500	539 ± 28	2.84	0.213	1021 ± 52 ± 55
2.1750	1840 ± 51	10.6	0.217	914 ± 26 ± 59
2.2000	2064 ± 54	13.7	0.218	791 ± 21 ± 54
2.2324	1508 ± 46	11.9	0.222	659 ± 20 ± 43
2.3094	1846 ± 51	21.1	0.223	452 ± 13 ± 30
2.3864	1601 ± 48	22.5	0.222	366 ± 11 ± 26
2.3960	4553 ± 80	66.9	0.222	352 ± 6 ± 19
2.5000	53.8 ± 8.2	1.10	0.228	247 ± 38 ± 18
2.6444	1335 ± 42	33.7	0.234	195 ± 6 ± 11
2.6464	1274 ± 41	34.1	0.233	184 ± 6 ± 12
2.7000	34.9 ± 6.5	1.03	0.238	163 ± 30 ± 10
2.8000	21.2 ± 6.3	1.01	0.239	101 ± 30 ± 7.0
2.9000	2096 ± 54	105	0.243	93.8 ± 2.4 ± 5.3
2.9500	302 ± 20	15.9	0.244	89.0 ± 5.8 ± 5.2
2.9810	254 ± 19	16.0	0.246	74.0 ± 5.5 ± 4.1
3.0000	256 ± 18	15.9	0.244	76.1 ± 5.3 ± 4.1
3.0200	268 ± 18	17.3	0.242	73.3 ± 5.0 ± 4.3
3.0800	1513 ± 40	126	0.223	61.8 ± 1.7 ± 4.1

Table 4
Summary of relative systematic uncertainties (in %) associated with the luminosity ($\mathcal{L}$), the tracking efficiency (Track), the photon detection efficiency (Photon), PID, branching fraction (Br), 4C kinematic fit (4C), background shape (Bkg), signal shape (Sig), fit range (Range), π^0 mass windows (m(π^0) and m(π^0_ω)), the initial state radiation and the vacuum polarization correction factor $(1+\delta)$ in the measurement of the Born cross section of the $e^+e^- \to \omega\pi^0$ process.

Ecm	$\mathcal{L}$	Track	Photon	PID	Br	4C	Bkg	Sig	Range	$m(\pi^0)$	$m(\pi^0_\omega)$	$(1+\delta)$	Total
2.0000	1.0	2.0	4.0	2.0	0.7	0.2	0.4	1.4	5.1	0.1	0.3	0.7	7.4
2.0500	1.0	2.0	4.0	2.0	0.7	0.3	0.4	0.3	4.4	0.4	0.4	0.6	6.8
2.1000	1.0	2.0	4.0	2.0	0.7	0.3	0.4	1.6	4.2	0.1	0.1	0.5	6.8
2.1250	1.0	2.0	4.0	2.0	0.7	0.3	0.2	1.1	4.2	0.1	0.1	0.5	6.7
2.1500	1.0	2.0	4.0	2.0	0.7	0.4	0.9	1.5	0.7	0.4	0.2	0.5	5.4
2.1750	1.0	2.0	4.0	2.0	0.7	0.4	0.0	0.4	4.1	0.0	0.2	0.5	6.6
2.2000	1.0	2.0	4.0	2.0	0.7	0.4	0.1	0.8	4.4	0.1	0.2	0.5	6.8
2.2324	1.0	2.0	4.0	2.0	0.7	0.4	0.1	0.8	3.9	0.2	0.3	0.5	6.5
2.3094	1.0	2.0	4.0	2.0	0.7	0.3	0.5	0.4	4.1	0.2	0.4	0.5	6.6
2.3864	1.0	2.0	4.0	2.0	0.7	0.3	1.4	0.9	4.7	0.3	0.4	0.5	7.1
2.3960	1.0	2.0	4.0	2.0	0.7	0.3	0.4	1.4	1.5	0.1	0.4	0.5	5.5
2.5000	1.0	2.0	4.0	2.0	0.7	0.4	0.4	2.4	4.2	1.3	1.0	0.5	7.2
2.6444	1.0	2.0	4.0	2.0	0.7	0.3	0.6	0.6	2.6	0.3	0.2	0.5	5.8
2.6464	1.0	2.0	4.0	2.0	0.7	0.1	0.9	1.4	3.4	0.5	0.3	0.5	6.4
2.7000	1.0	2.0	4.0	2.0	0.7	0.6	2.7	1.5	2.9	1.2	1.4	0.5	6.9
2.8000	1.0	2.0	4.0	2.0	0.7	0.1	0.2	1.6	2.1	0.7	0.9	0.5	5.8
2.9000	1.0	2.0	4.0	2.0	0.7	0.6	1.1	1.7	1.2	0.2	0.6	0.5	5.7
2.9500	1.0	2.0	4.0	2.0	0.7	0.2	0.5	1.2	2.3	0.7	0.2	0.5	5.8
2.9810	1.0	2.0	4.0	2.0	0.7	0.3	0.4	1.9	0.5	0.1	0.8	0.5	5.5
3.0000	1.0	2.0	4.0	2.0	0.7	0.4	0.3	0.5	1.4	0.7	0.6	0.5	5.4
3.0200	1.0	2.0	4.0	2.0	0.7	0.2	0.6	1.2	2.1	1.2	0.8	0.5	5.8
3.0800	1.0	2.0	4.0	2.0	0.7	0.5	0.8	1.7	3.5	1.1	0.8	0.5	6.6

4. Line shape analysis

4.1. Analysis of the $e^+e^- \to \omega\eta$ process

To study possible resonant structures in $e^+e^- \to \omega\eta$, a maximum likelihood fit of the type used in Ref. [61] is performed to the dressed cross sections, which are the products of Born cross sections and VP factors. Previous results from the SND [55] and CMD3 [56] collaborations are also included to be able to describe the low-energy behavior of the cross section, while BaBar's result is not used due to their large uncertainties or non-observation without uncertainty. In the fit, a possible resonant amplitude is parameterized using a Breit-Wigner function with a mass-independent width. The flat contribution in the c.m. energy region between 2 and 3 GeV dominantly stems from tails of the $\omega(1420)$ and $\omega(1650)$ (or $\phi(1680)$) resonances. Following Ref. [55], the dressed cross section is modeled as

$$\sigma(s) = \frac{12\pi}{s^{\frac{3}{2}}}\left|f_1 - f_2 + e^{i\varphi} f_3\right|^2 P_f(s), \qquad (2)$$

where $f_R = \sqrt{\frac{\Gamma_R^{ee}\cdot B_R^{\omega\eta}}{P_f(m_R)}}\frac{m_R^{3/2}\sqrt{\Gamma_R}}{s-m_R^2+i\sqrt{s}\Gamma_R}$ (here $R = 1,2,3$ is an index for the resonance) describes the resonant contributions from the $\omega(1420)$, $\omega(1650)$ (or $\phi(1680)$) and $Y(2180)$ (referring to the structure around $\sqrt{s} = 2.2$ GeV) and $\Gamma_R^{ee}\cdot B_R^{\omega\eta}$ is the product of the electronic width of the resonance R and the branching fraction of the $R \to \omega\eta$ decay. Furthermore, m_R and Γ_R are the mass and width of the resonance R, and φ is the relative phase angle of the f_3 contribution relative to the $f_1 - f_2$ contribution. The phase space factor $P_f(s)$ is given by $P_f(s) = q^3$, where q is the ω momentum in the e^+e^- c.m. frame calculated for the mass value $m(\omega) = 0.78265\,\text{GeV}/c^2$ given in Ref. [1]. The free fit parameters are taken as $\Gamma^{ee}\cdot B_1^{\omega\eta}$, m_2, Γ_2, $\Gamma^{ee}\cdot B_2^{\omega\eta}$, m_3, Γ_3, $\Gamma^{ee}\cdot B_3^{\omega\eta}$ and φ. The m_1 and Γ_1 values are fixed to the values determined by the SND Collaboration [55], since the significance of the $\omega(1420)$ resonance is not large enough at the given c.m. energies. In the fit, uncertainties from previous experiments are considered uncorrelated, while the uncertainties derived in this work are split into the uncorrelated and the correlated contributions. The former contributions include those stemming from the choice of signal and background shape as well as fit range and the treatment of peaking backgrounds whereas the latter include the remaining systematic uncertainties. Fig. 4 and Table 5 show the results from our fit. Two solutions are found with the same fit quality of $\chi^2/\text{ndf} = 79/67$, where ndf is the number of degrees of freedom. The significance of the third resonance is determined by comparing the change of the goodness (χ^2) in a fit without the third resonance and considering the change of the ndf. Solution I corresponds to constructive interference between the f_3 amplitude and the remaining $f_1 - f_2$ contribution, while solution II corresponds to the case of destructive interference. The two solutions share all parameters other than those given in Table 5. Among the other free parameters, the mass and width of f_2 are determined to be 1670 ± 4 MeV/c^2 and 124 ± 7 MeV, respectively, with $\Gamma^{ee}\cdot B_{f_2}^{\omega\eta}$ equal to 54 ± 2 eV.

Table 5
Resonance parameters of the $Y(2180)$ as obtained in the fit to the $e^+e^- \to \omega\eta$ dressed cross section.

Parameters	Solution I	Solution II
$m_{Y(2180)}$ (MeV/c^2)	2176 ± 24	
$\Gamma_{Y(2180)}$ (MeV)	89 ± 50	
$\Gamma^{ee}\cdot B^{\omega\eta}$ (eV)	0.43 ± 0.15	1.25 ± 0.48
φ	2.6 ± 0.3	1.9 ± 0.2
significance	6.2σ	

4.2. Analysis of the $e^+e^- \to \omega\pi^0$ process

A fit is performed to the dressed cross sections of $e^+e^- \to \omega\pi^0$ using a similar method as described in Sec. 4.1. Previous results from the SND collaboration [43,44] are included in order to provide the low-energy contributions that will only appear as tails in the energy region under study. BaBar's result is not used since there is an obvious bias compared to the result in this work in the overlap region, and others are not used due to their large uncertainties. Here, the fit model is parameterized as a coherent sum of four Breit-Wigner functions,

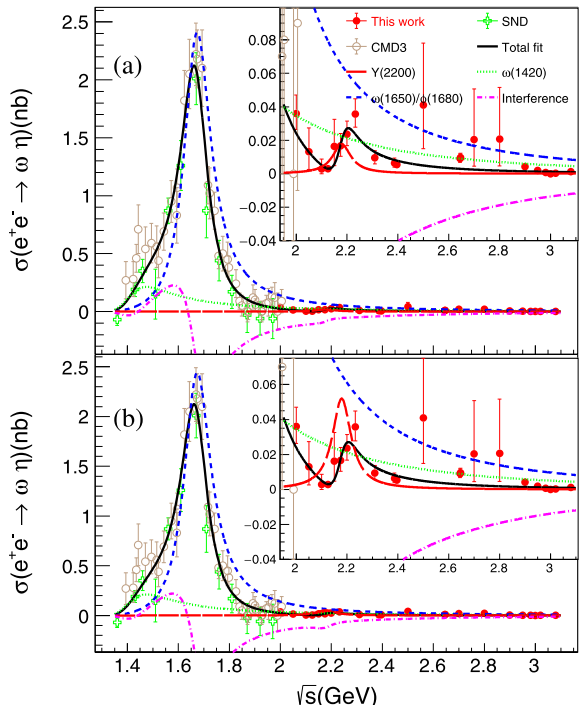

Fig. 4. Fit to the dressed cross sections of $e^+e^- \to \omega\eta$. (a) Solution I. (b) Solution II. (Red) filled circles represent the data from this work, whereas (brown) open circles show the data from CMD3 and the (green) open crosses the data from SND. The (black) solid curves are the total fit results, the (red) long-dashed curves indicate the $Y(2180)$ resonance contribution, the (blue) short-dashed curves represent the $\omega(1650)$ or $\phi(1680)$ contribution, the (green) dotted curves display the $\omega(1420)$ contribution and (magenta) dotted-dashed curves show the interference contribution. In the upper right panel of both (a) and (b), a zoom into the region of the $Y(2180)$ resonance is shown.

$$\sigma(s) = \frac{12\pi}{s^{\frac{3}{2}}}\left|f_1 + e^{i\varphi_1} f_2 + e^{i\varphi_2} f_3 + e^{i\varphi_3} f_4\right|^2 P_f(s), \tag{3}$$

where f_R (with $R = 1, 2, 3, 4$) are the Breit-Wigner functions for the $\rho(770)$, $\rho(1450)$, $\rho(1700)$ and $Y(2040)$ (referring to the structure around $\sqrt{s} = 2.040$ GeV) resonances, which take the same form as described in Eq. (2) except for the $\rho(770)$. Since the mass of the $\rho(770)$ resonance is below the $\omega\pi^0$ threshold, we instead use $f_{\rho(770)} = \frac{A}{s - m^2_{\rho(770)} + i\sqrt{s}\Gamma_{\rho(770)}(s)}$. The formula for the energy-dependent width $\Gamma_{\rho(770)}(s)$ is given in Ref. [42]. The free fit parameters are taken as A, $\Gamma_{\rho(1450)}$, $\Gamma_{\rho(1700)}$, $m_{Y(2040)}$, $\Gamma_{Y(2040)}$, $\Gamma^{ee}_R \cdot B^{\omega\eta}_R$ and φ_R.

The masses of the $\rho(1450)$ and $\rho(1700)$ resonances are fixed to the average values as given by the PDG [1]. In the fit, a possible effect of omitting other data available in the literature on the results obtained in this work is studied and will be discussed in Sec. 4.3. Correlated and uncorrelated uncertainties of the present work are incorporated in the same way as described in Sec. 4.1, while the uncertainties of the previous experiments are considered uncorrelated.

The fit shown in Fig. 5 finds a resonance with a mass of $(2034 \pm 13)\,\mathrm{MeV}/c^2$, width of $(234 \pm 30)\,\mathrm{MeV}$ and $\Gamma^{ee} \cdot B^{\omega\pi^0}$ of (34 ± 11) eV with a fit quality of $\chi^2/\mathrm{ndf} = 128/90$. The significance of the $Y(2040)$ contribution is found to be larger than 10σ.

4.3. Systematic uncertainties

The systematic uncertainties of the resonant parameters in the fit to the Born cross sections of $e^+e^- \to \omega\eta$ include contributions from the determination of the c.m. energy and the energy spread, fixed parameters in the fit, and the data from other experiments

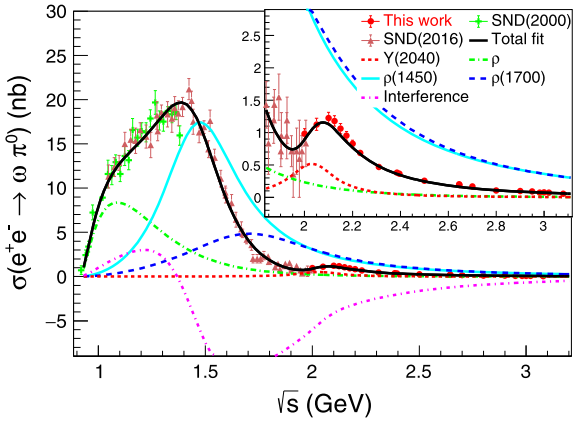

Fig. 5. Fit to the dressed cross sections of the $e^+e^- \to \omega\pi^0$ process. (Red) filled circles correspond to the data obtained in this work, while (brown) filled triangles and (green) filled crosses are the data from SND. The (black) solid curve is the total fit result, the (red) dashed curve is the $Y(2040)$ contribution, the (blue) long-dashed curve is the contribution from the $\rho(1700)$, the (light blue) dotted-dotted-dashed curve stems from the $\rho(1450)$, the (green) dotted-dashed curve corresponds to the $\rho(770)$ and the (magenta) dotted curve is the interference contribution.

that is included in the fit. The uncertainty of the c.m. energy from BEPCII is small and found to be negligible comparing to the statistic uncertainty in the determination of the resonance parameters. The effect resulting from fixing the parameters of the $\omega(1420)$ resonance is studied by varying the mass and width within the uncertainties quoted in the PDG [1] and yields an uncertainty of $\Delta m = 3\,\mathrm{MeV}/c^2$, $\Delta\Gamma = 5\,\mathrm{MeV}$ and $\Delta(\Gamma^{ee} \cdot B^{\omega\eta})$ equal to 0.03 eV for solution I and 0.16 eV for solution II.

We distinguish between two different types of systematic uncertainties, those that are uncorrelated between the different center-of-mass energies and those that are correlated. While the uncorrelated uncertainties are included in the fit to the cross section, the correlated uncertainties that are common for all center-of-mass energies ($\sim 6\%$) only affect the $\Gamma^{ee} \cdot B^{\omega\eta}$ measurement and we find a resulting systematic uncertainty of 0.03 eV for solution I and 0.09 eV for solution II. Assuming all sources of systematic uncertainties are uncorrelated and thus adding them in quadrature, the total systematic uncertainty is $3\,\mathrm{MeV}/c^2$ for the mass, 5 MeV for the width, 0.04 eV (solution I) or 0.18 eV (solution II) for $\Gamma^{ee} \cdot B^{\omega\eta}$ of the $Y(2180)$.

For the systematic uncertainties of the resonant parameters of the $Y(2040)$ in $e^+e^- \to \omega\pi^0$, the contribution introduced by taking the data points of other experiments into account in the fit is significant. It is investigated by including all available measurements [42–49] and comparing with the nominal fit result above. Other uncertainties are considered in the same way as stated before for the $Y(2180) \to \omega\eta$ case. All sources of systematic uncertainties are added in quadrature, obtaining the total systematic uncertainty of $9\,\mathrm{MeV}/c^2$ for the mass, 25 MeV for the width and 16 eV for $\Gamma^{ee} \cdot B^{\omega\pi^0}$ of the observed $Y(2040)$. Since the resonances in $e^+e^- \to \omega\pi^0$ line shape are from the excited ρ states, which are wider than those in the $\omega\eta$ line shape, the contribution from other resonances and the interferences lead to larger systematic uncertainties in the resonant parameters of the $Y(2040)$ state.

5. Summary and discussion

The Born cross sections of the $e^+e^- \to \omega\eta$ and $e^+e^- \to \omega\pi^0$ processes have been measured at $\sqrt{s}$ from 2.000 to 3.080 GeV. They are consistent with most of previous measurements in the overlap region, but deviate with BaBar's results, especially in the $\omega\pi^0$ process. Two resonant structures are observed in the mea-

sured line shapes. One resonant structure is observed with a significance of 6.2σ in the cross section of the $e^+e^- \to \omega\eta$ process, with mass $m = (2176 \pm 24 \pm 3)\,\mathrm{MeV}/c^2$, width $\Gamma = (89 \pm 50 \pm 5)\,\mathrm{MeV}$, and $\Gamma^{ee} \cdot B^{\omega\eta} = (0.43 \pm 0.15 \pm 0.04)$ eV or $(1.25 \pm 0.48 \pm 0.18)$ eV, depending on the choice between two ambiguous fit solutions. The observed structure agrees well with the properties of the $\phi(2170)$ resonance, which indicates the first observation of the decay $\phi(2170) \to \omega\eta$.

Another structure is observed in the $\omega\pi^0$ cross section with a significance of more than 10σ and with a mass of $m = (2034 \pm 13 \pm 9)\,\mathrm{MeV}/c^2$, width of $\Gamma = (234 \pm 30 \pm 25)\,\mathrm{MeV}$ and $\Gamma^{ee} \cdot B^{\omega\pi^0}$ of $(34 \pm 11 \pm 16)$ eV. This structure could either be the $\rho(2000)$ or the $\rho(2150)$ state. However, the mass and width of the observed resonance is closer to the $\rho(2000)$ resonance, which is suggested to be the 2^3D_1 state [41].

Declaration of competing interest

The authors declare that they have no known competing financial interests or personal relationships that could have appeared to influence the work reported in this paper.

Acknowledgements

The BESIII collaboration thanks the staff of BEPCII, the IHEP computing center and the supercomputing center of USTC for their strong support. This work is supported in part by National Key Basic Research Program of China under Contract Nos. 2015CB856700, 2020YFA0406400; National Natural Science Foundation of China (NSFC) under Contracts Nos. 11335008, 11375170, 11475164, 11475169, 11625523, 11605196, 11605198, 11635010, 11705192, 11735014, 11822506, 11835012, 11935015, 11935016, 11935018, 11950410506, 11961141012, 12035013; the Chinese Academy of Sciences (CAS) Large-Scale Scientific Facility Program; Joint Large-Scale Scientific Facility Funds of the NSFC and CAS under Contracts Nos. U1532102, U1732263, U1832103, U1832207, U2032111; CAS Key Research Program of Frontier Sciences under Contracts Nos. QYZDJ-SSW-SLH003, QYZDJ-SSW-SLH040; 100 Talents Program of CAS; INPAC and Shanghai Key Laboratory for Particle Physics and Cosmology; ERC under Contract No. 758462; German Research Foundation DFG under Contracts Nos. Collaborative Research Center CRC 1044, FOR 2359; Istituto Nazionale di Fisica Nucleare, Italy; Ministry of Development of Turkey under Contract No. DPT2006K-120470; National Science and Technology fund; STFC (United Kingdom); The Knut and Alice Wallenberg Foundation (Sweden) under Contract No. 2016.0157; The Royal Society, UK under Contracts Nos. DH140054, DH160214; The Swedish Research Council; U.S. Department of Energy under Contracts Nos. DE-FG02-05ER41374, DE-SC-0012069.

References

[1] P.A. Zyla, et al., Particle Data Group, Prog. Theor. Exp. Phys. 2020 (2020) 083C01.
[2] G.J. Ding, M.L. Yan, Phys. Lett. B 650 (2007) 390.
[3] J. Ho, R. Berg, T.G. Steele, Phys. Rev. D 100 (2019) 034012.
[4] G.J. Ding, M.L. Yan, Phys. Lett. B 657 (2007) 49.
[5] C.Q. Pang, Phys. Rev. D 99 (2019) 074015.
[6] C.G. Zhao, et al., Phys. Rev. D 99 (2020) 114014.
[7] Q. Li, et al., arXiv:2004.05786.
[8] Z.G. Wang, Nucl. Phys. A 791 (2007) 106.
[9] C.R. Deng, J.L. Ping, T. Goldman, Phys. Rev. D 82 (2010) 074001.
[10] S.S. Agaev, K. Azizi, H. Sundu, Phys. Rev. D 101 (2020) 074012.
[11] H.W. Ke, X.Q. Li, Phys. Rev. D 99 (2019) 036014.
[12] R.R. Dong, et al., Eur. Phys. J. C 80 (2020) 749.
[13] F.X. Liu, et al., arXiv:2008.01372.
[14] L. Zhao, et al., Phys. Rev. D 87 (2013) 054034.
[15] E. Klempt, A. Zaitsev, Phys. Rep. 454 (2007) 1.
[16] Y.L. Yang, D.Y. Chen, Z. Lu, Phys. Rev. D 100 (2019) 073007.
[17] A.M. Torres, et al., Phys. Rev. D 78 (2008) 074031.
[18] L. Alvarez-Ruso, J.A. Oller, J.M. Alarcón, Phys. Rev. D 80 (2009) 054011.
[19] T. Barnes, N. Black, P.R. Page, Phys. Rev. D 68 (2003) 054014.
[20] Y. Dong, et al., Phys. Rev. D 96 (2017) 074027.
[21] S.S. Agaev, K. Azizi, H. Sundu, Phys. Rev. D 101 (2020) 074012.
[22] B. Aubert, et al., BABAR Collaboration, Phys. Rev. D 74 (2006) 091103(R).
[23] M. Ablikim, et al., BES Collaboration, Phys. Rev. Lett. 100 (2008) 102003.
[24] M. Ablikim, et al., BESIII Collaboration, Phys. Rev. D 91 (2015) 052017.
[25] C.P. Shen, et al., Belle Collaboration, Phys. Rev. D 80 (2009) 031101(R).
[26] J.P. Lees, et al., BABAR Collaboration, Phys. Rev. D 86 (2012) 012008.
[27] M. Ablikim, et al., BESIII Collaboration, Phys. Rev. Lett. 124 (2020) 112001.
[28] M. Ablikim, et al., BESIII Collaboration, Phys. Rev. D 99 (2019) 032001.
[29] D.Y. Chen, J. Liu, J. He, Phys. Rev. D 101 (2020) 074045.
[30] M. Ablikim, et al., BESIII Collaboration, Phys. Rev. D 102 (2020) 012008.
[31] M. Ablikim, et al., BESIII Collaboration, Phys. Rev. D 100 (2019) 032009.
[32] C.Q. Pang, et al., Phys. Rev. D 101 (2020) 074022.
[33] A. Hasan, D.V. Bugg, Phys. Lett. B 334 (1994) 215.
[34] D.V. Bugg, Phys. Rep. 397 (2004) 257.
[35] J.P. Lees, et al., BABAR Collaboration, Phys. Rev. D 101 (2012) 012011.
[36] J.P. Lees, et al., BABAR Collaboration, Phys. Rev. D 86 (2012) 032013.
[37] B. Aubert, et al., BABAR Collaboration, Phys. Rev. D 76 (2007) 092005.
[38] M.E. Biagini, S. Dubnicka, E. Etim, Il Nuovo Cimento A 104 (3) (1991).
[39] A.B. Clegg, A. Donnachie, Z. Phys. C, Part. Fields 45 (1990) 677.
[40] L.M. Wang, J.Z. Wang, X. Liu, Phys. Rev. D 102 (2020) 034037.
[41] L.P. He, X. Wang, X. Liu, Phys. Rev. D 88 (2013) 034008.
[42] M.N. Achasov, et al., SND Collaboration, Phys. Lett. B 486 (2000) 29.
[43] M.N. Achasov, et al., SND Collaboration, J. Exp. Theor. Phys. 96 (2003) 789.
[44] M.N. Achasov, et al., SND Collaboration, Phys. Rev. D 94 (2016) 112001.
[45] S.I. Dolinsky, et al., ND Collaboration, Phys. Lett. B 174 (1986) 453.
[46] R.R. Akhmetshin, et al., CMD-2 Collaboration, Phys. Lett. B 466 (1999) 392.
[47] R.R. Akhmetshin, et al., CMD-2 Collaboration, Phys. Lett. B 562 (2003) 173.
[48] D. Bisello, et al., DM2 Collaboration, Orsay preprint LAL 90-35 (1990), in: International Conference on High Energy Physics, Singapore, 1990.
[49] J.P. Lees, et al., BABAR Collaboration, Phys. Rev. D 96 (2017) 092009.
[50] M. Ablikim, et al., BESIII Collaboration, Nucl. Instrum. Methods A 614 (2010) 345.
[51] C.H. Yu, et al., in: Proceedings of IPAC2016, Busan, Korea, 2016.
[52] S. Agostinelli, et al., GEANT4 Collaboration, Nucl. Instrum. Methods A 506 (2003) 250.
[53] Z.Y. Deng, et al., Chin. Phys. C 30 (2006) 371.
[54] R.G. Ping, Chin. Phys. C 38 (2014) 083001.
[55] M.N. Achasov, et al., SND Collaboration, Phys. Rev. D 94 (2016) 092002.
[56] R.R. Akhmetshin, et al., CMD-3 Collaboration, Phys. Lett. B 773 (2017) 150.
[57] B. Aubert, et al., BABAR Collaboration, Phys. Rev. D 73 (2006) 052003.
[58] M. Ablikim, et al., BESIII Collaboration, Chin. Phys. C 41 (2017) 063001.
[59] W.L. Yuan, et al., Chin. Phys. C 40 (2016) 026201.
[60] M. Ablikim, et al., BESIII Collaboration, Phys. Rev. D 87 (2013) 012002.
[61] M. Ablikim, et al., BESIII Collaboration, Phys. Rev. Lett. 118 (2017) 092002.